A NOVEL GPS FAULT DETECTION AND EXCLUSION ALGORITHM AIDED BY IMU AND VO DATA FOR VEHICLE INTEGRATED NAVIGATION IN URBAN ENVIRONMENTS

Yuanyuan Wang, Rui Sun*

the Key Laboratory of Maritime Intelligent Cyberspace Technology (Nanjing University of Aeronautics and Astronautics), Ministry of Education, Nanjing, China, rui.sun@nuaa.edu.cn

KEY WORDS: GPS, IMU, VO, FDE, Predicted pseudorange error, Hierarchical clustering.

ABSTRACT:

High accuracy positioning is crucial for various applications that require accurate and reliable positioning data, such as autonomous vehicles (AVs), agriculture, and intelligent transportation. Global Positioning System (GPS) is widely used in integration with Inertial Measurement Unit (IMU) and Visual Odometry (VO) to implement an accurate and robust navigation system. However, the performance of the integrated system can be severely degraded in urban environments due to non-line-of-sight (NLOS) reception and multipath interference. To overcome these challenges, a novel Fault Detection and Exclusion (FDE) algorithm aided with IMU and VO measurements is proposed to identify and isolate the contaminated satellite signals. The algorithm utilizes instantaneous measurements from IMU and VO to predict the current vehicle position, enabling the estimation of pseudorange errors in GPS measurements. A FDE algorithm based on Hierarchical clustering is then developed to identify GPS signals with significant errors based on the predicted pseudorange error. An experimental field test was conducted using a land vehicle to evaluate the effectiveness of the proposed algorithm. The results show that the GPS/IMU/VO integrated navigation system with the proposed FDE algorithm has significantly improved the positioning accuracy and reliability compared to the traditional system. The proposed algorithm achieves a positioning accuracy with a 3D Root Mean Square Error (RMSE) of 11.18m in urban environment, making an improvement of 68.2% over the traditional GPS/IMU/VO integrated navigation system.

1. INTRODUCTION

Autonomous vehicles (AVs) have emerged as key contributors to enhancing passenger safety and reducing overall operating costs (Fagnant and Kockelman, 2015). However, the implementation of AVs also brings significant challenges, particularly in terms of providing accurate, continuous, and reliable vehicle positioning information. The global navigation satellite systems (GNSS), such as global positioning system (GPS), can provide long-term absolute positioning information in open sky environments, often integrated with other sensors, such as inertial measurement units (IMU) and vision sensors for vehicle positioning. However, GNSS signals are easily blocked, diffracted or reflected by tall buildings in harsh urban environments, resulting in non-line-of-sight (NLOS) reception and multipath interference (MI) (Chen et al., 2020). Notably, NLOS reception can cause significant pseudorange errors, impacting the positioning accuracy and reliability of GNSS and the integrated navigation system (MacGougan et al., 2002). Therefore, fault detection and exclusion (FDE) is crucial for AVs to achieve high levels of positioning accuracy and reliability in urban environments.

One of the most representative FDE algorithms is the Receiver Autonomous Integrity Monitoring (RAIM) algorithm (Feng et al., 2006). The classic RAIM algorithm is aimed to ensure the integrity of GNSS positioning solution by checking the consistency of GNSS measurements, identifying and excluding faulty satellite measurements. The conventional RAIM algorithms include the pseudorange comparison method (Lee, 1986), the least squares residual method (Parkinson and Axelrad, 1988), and the parity vector method (Sturza, 1988). These three algorithms have been proved equivalent, when the noise follows a Gaussian distribution. But they only perform effective FDE performance in single-fault situations. With the rapid developments of multi-constellation GNSS technology, the possibility of multiple satellites malfunctioning simultaneously is also increasing. Blanch et al. proposed an advanced RAIM (ARAIM) method based on multiple hypothesis solution separation to detect multiple faults (Blanch et al., 2012). However, the methods exist substantial computational burden when assessing the consistency across numerous subsets. These RAIM algorithms can work well in aviation settings where exist measurement redundancy. However, the algorithms are difficult to directly transferable to dynamic applications in urban areas due to the limited satellite availability and poor satellite geometrical configurations. Moreover, RAIM is susceptible to errors in the initial position estimation, as inaccurate or biased estimates can result in incorrect fault detection and exclusion, thereby compromising the reliability of the FDE process.

Moreover, to mitigate pseudorange measurement errors in GNSS positioning, machine learning methods have also been employed to identify and exclude NLOS/multipath signals by considering the factors that influence measurement errors such as the carrier to noise ratio, elevation angle, pseudorange residuals, and other derivatives or their combinations. Hsu trained a classifier using support vector machine (SVM) to classify GNSS signal types into three categories, LOS, multipath interference and NLOS (Hsu, 2017). The features he selected include carrier to noise ratio, change rate of carrier to noise ratio, pseudorange residue, difference between delta pseudorange and pseudorange rate. The experiment result shows that the proposed algorithm can achieve a classification accuracy of 75%. GUERMAH et al. exploited the potential of right-hand circular polarized (RHCP) and left-hand circular polarized (LHCD) for signal processing and proposed an improved GNSS signal classifier using information provided by

RHCP and LHCP antennas (C/N0-R-L and satellite elevation) and Decision Trees technique (GUERMAH et al. 2018). The results show that the proposed algorithm can give an accuracy of 99%. Sun et al. tested the classification algorithm based on gradient boosting decision tree (GBDT), decision tree, distance weighted k-nearest neighbour (KNN) and adaptive network-based fuzzy inference system (ANFIS), using the features of C/N0, pseudorange residuals and satellite elevation angle (Sun et al., 2020). The results show that the GBDT based algorithm achieves the best classification accuracy. The proposed GBDT algorithm with NLOS detection and exclusion can provide a positioning accuracy improvement of 34.1% compared to the traditional method. These algorithms all belong to the supervised learning methods and the classification accuracy is closely related to the accuracy of the labelled training sets. However, it is difficult and costly to obtain accurate labelled training sets.

Multi sensor fusion methods have also been proposed to improve the positioning accuracy by detecting and eliminating faulty GNSS signals. Meguro et al. proposed a precise positioning technique that utilizes an omnidirectional infrared camera to eliminate invisible satellites (Meguro et al., 2009). The effectiveness of this technique was evaluated through static and kinematic experiments, and the results confirmed its effectiveness. However, the high cost associated with this approach limits its widespread use. Peyraud employed a 3D urban model to predict visible satellites and then eliminated potential faulty satellites to mitigate multipath effects (Pevraud et al., 2013). While this algorithm improves positioning accuracy, it is computationally complex and cannot achieve real-time processing. Additionally, Sun et al. proposed a FDE algorithm that utilizes a sliding window and a detector (Sun et al., 2021). This algorithm is based on pseudorange comparison using IMU data and GNSS pseudorange measurements. Experimental results demonstrate that the proposed algorithm enhances positioning accuracy compared to scenarios without fault exclusion, particularly in mid and urban canyons.

As discussed above, although several methods have demonstrated effectiveness in mitigating multipath effects, they also have some limitations. Additionally, these FDE methods may degrade satellite geometric distribution and may not be suitable for low-visibility areas. IMU provides high short precision and is unaffected by the external environments. It can be integrated with GNSS to complement each other and achieve enhanced accuracy and robustness. However, during extended GNSS signal outages, positioning accuracy can deteriorate rapidly. To overcome these challenges, we design a novel GPS FDE algorithm that utilizes IMU and Visual Odometry (VO) data to improve the vehicle navigation performance in urban environments. The algorithm predicts pseudorange errors based on current IMU and VO measurements and employs Hierarchical Clustering method to identify faulty satellite signals considering the predicted pseudorange errors.

The remainder of this paper is organized as follows: Section 2 introduces the proposed algorithm, Section 3 provides experimental verification, and finally, Section 4 concludes the paper.

2. ALGORITHM DESIGN

2.1 Algorithm Framework

The framework of the proposed GPS FDE algorithm, aided by IMU and VO data for vehicle integrated navigation in urban environments, is depicted in Figure 1. In the first step, the current vehicle velocities are estimated using camera and IMU data, respectively. Based on the previous vehicle position estimated by the loosely integrated GPS/IMU/VO navigation system, we can predict the current vehicle position. Next, utilizing the predicted vehicle position and GPS observations, we can estimate pseudorange errors. Considering these predicted pseudorange errors, we employ the Hierarchical Clustering algorithm to identify GPS signals that exhibit consistency, thereby excluding inconsistent satellite signals. This process facilitates the estimation of position and velocity using the remaining reliable GPS measurements. Finally, we obtain the loosely integrated navigation solution by combining the estimates from the GPS measurements with the information derived from the IMU and VO data. This integrated system can offer a more robust estimation of the vehicle's position and velocity in urban environments.

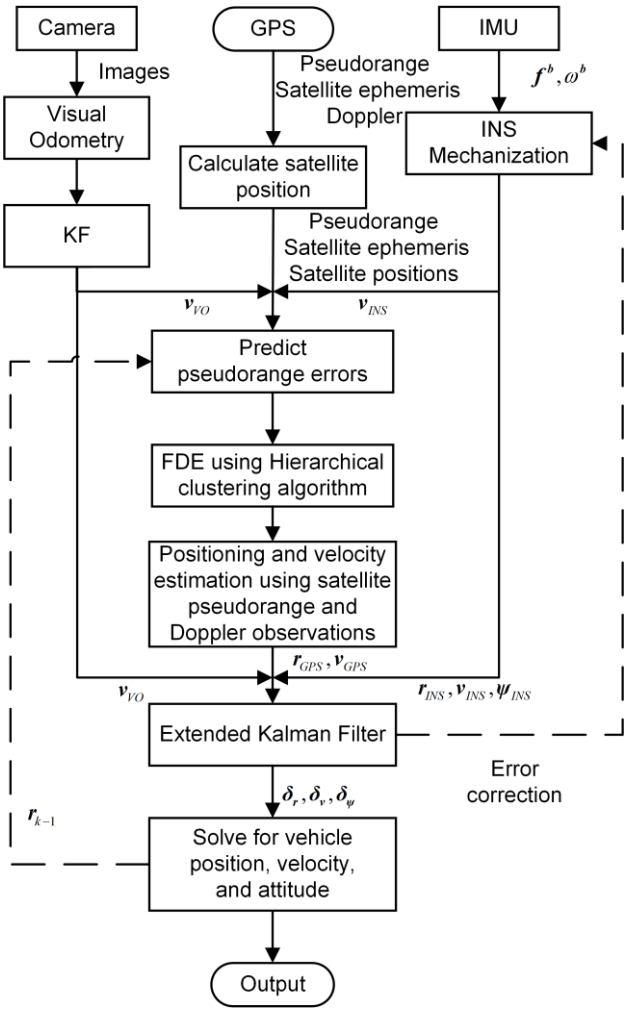

Figure 1. The algorithm framework of the proposed method

2.2 IMU and VO Data Based Vehicle Position Prediction

GPS signals are easily contaminated by external factors, such as interference, noise, which can compromise the accuracy and reliability of GPS positioning results. Consequently, incorrect FDE may occur. Fortunately, we can enhance the accuracy and reliability of position estimation by utilizing the IMU and VO data.

The IMU provides instantaneous measurements of linear acceleration and angular velocity, making it immune to external interference. By applying a mechanical arrangement algorithm,

we can utilize these measurements to calculate the vehicle velocity $\boldsymbol{v}_{IMU\_k}^{b}$.

In addition, the camera used in the VO system can capture a larger number of features in urban environments, offering valuable visual information for position estimation. Through techniques such as feature extraction, feature matching, and VO, we can determine the vehicle position in the camera frame. To integrate this information with the IMU data, we then convert the position to the body frame.

$$\boldsymbol{t}_{raw\_VO}^{b} = \boldsymbol{C}_{c}^{b}\boldsymbol{t}_{raw\_VO}^{c} + \boldsymbol{t}_{c}^{b} \tag{1}$$

where, $\boldsymbol{t}_{raw\_VO}^{c}$ and $\boldsymbol{t}_{raw\_VO}^{b}$ are raw vehicle position calculated by VO in the camera frame and body frame, respectively. $\boldsymbol{C}_{c}^{b}$ is the rotation matrix from the camera frame to the body frame obtained by calibration. $\boldsymbol{t}_{c}^{b}$ is the translation vector from the camera frame to the body frame.

To estimate the vehicle velocity, a Kalman filter (KF) with a constant acceleration model is designed. The velocity estimation takes into account the non-holonomic Constraint (NHC) (Yang et al. 2016), which considers the vehicle stability in both lateral and vertical directions.

$$\boldsymbol{v}_{VO\_k}^{b} = \begin{bmatrix} v_{VO\_k}^{bx} \\ 0 \\ 0 \end{bmatrix} \tag{2}$$

where, $\boldsymbol{v}_{VO\_k}^{b}$ is the vehicle velocity calculated by VO at time epoch k with NHC. $v_{VO\_k}^{bx}$ represents the vehicle forward velocity component in the body frame calculated by the KF.

By integrating the estimated velocities, we can predict the current vehicle position in the Earth-Centered, Earth-Fixed (ECEF) frame with the vehicle position calculated by the integrated navigation system at the previous epoch.

$$\boldsymbol{r}_{pre\_k} = \boldsymbol{r}_{k-1} + \frac{1}{2}\boldsymbol{C}_{n}^{e}\boldsymbol{C}_{b}^{n}(\boldsymbol{v}_{VO\_k}^{b} + \boldsymbol{v}_{IMU\_k}^{b})t \tag{3}$$

where $\boldsymbol{r}_{pre\_k}$ is the predicted current vehicle position in the ECEF frame, $\boldsymbol{r}_{k-1}$ is the previous vehicle position calculated by the integrated navigation system, $\boldsymbol{C}_{b}^{n}$ is the state transition matrix from the body frame to the navigation frame, $\boldsymbol{C}_{n}^{e}$ is the state transition matrix from the navigation frame to the ECEF frame, t is the time interval between time epoch k-1 to time epoch k.

2.3 Pseudorange Errors Prediction

The pseudorange measured between the user receiver and the satellite is:

$$\rho = r + c\left(t^{u} - t^{s}\right) + D^{trop} + D^{iono} + \varepsilon \tag{4}$$

where, r is the geometric distance between the satellite and the user receiver; c is the speed of light; t^{u} is the receiver clock error; t^{s} is the satellite clock error, which can be corrected according to the broadcast ephemeris; D^{trop} and D^{iono} is delays in the troposphere and ionosphere, which can be corrected by the Saastamoinen model and Klobuchar model, ε mainly contains NLOS and multipath errors.

The pseudorange observation obtained by the correction of satellite clock error, troposphere and ionosphere delay, is:

$$\rho^{c} = r + c\left(t^{u} - \Delta t^{s}\right) + \Delta D^{trop} + \Delta D^{iono} + \varepsilon \tag{5}$$

where Δt^{s}, ΔD^{trop}, and ΔD^{iono} are residuals after correction.

The pseudorange error can be obtained:

$$\Delta\rho = \rho^{c} - r = c\left(t^{u} - \Delta t^{s}\right) + \Delta D^{trop} + \Delta D^{iono} + \varepsilon \tag{6}$$

where, $\Delta\rho$ is pseudorange error.

To predict the pseudorange error, we calculate the geometric distance between the satellite and the user receiver according to the vehicle position predicted by IMU and VO data.

$$r_{pre} = \sqrt{\left(x_{s}^{i} - x_{pre}^{e}\right)^{2} + \left(y_{s}^{i} - y_{pre}^{e}\right)^{2} + \left(z_{s}^{i} - z_{pre}^{e}\right)^{2}} \tag{7}$$

where r_{pre} is the predicted geometric distance between the satellite and the vehicle; $\left(x_{s}^{i}, y_{s}^{i}, z_{s}^{i}\right)$ is the coordinate of the *i*-th satellite in the ECEF frame, $\left(x_{pre}^{e}, y_{pre}^{e}, z_{pre}^{e}\right)$ is the coordinate of the $\boldsymbol{r}_{pre\_k}$.

Then we can predict the pseudorange error:

$$\Delta\rho_{pre} = \rho^{c} - r_{pre} = c\left(t^{u} - \Delta t^{s}\right) + \Delta D^{trop} + \Delta D^{iono} + \varepsilon \tag{8}$$

where, $\Delta\rho_{pre}$ is the predicted pseudorange error.

2.4 FDE Using the Hierarchical Clustering Algorithm

Regarding the predicted pseudorange errors, the receiver clock errors remain consistent across all satellites, while the residual errors are generally small when compared to NLOS and multipath errors. NLOS signals arise when satellite signals encounter reflection during transmission, yielding larger predicted pseudorange errors compared to Line-of-Sight (LOS) signals. Multipath interference, which encompasses both direct and reflected signals, engenders predicted pseudorange errors that can exceed or below those of LOS signals. Consequently, the predicted pseudorange errors for NLOS and multipath signals diverge from those of LOS signals and are contingent upon the traits of signal propagation pathways.

Based on this understanding, we design a Fault Detection and Exclusion (FDE) method that incorporates the hierarchical clustering (Nielsen, 2016) algorithm to classify satellite signals into three clusters.

In this process, the predicted pseudorange error is chosen as the feature, and the Euclidean distance is selected as the distance metric. The hierarchical clustering algorithm is applied using this distance metric, starting with each satellite signal as an individual cluster. Iteratively, the clusters are merged based on their similarity until the three clusters are obtained. The cluster center of the cluster with the highest number of samples represents the predicted pseudorange error without NLOS and multipath errors since LOS signals should be consistent.

Next, we compare all the predicted pseudorange errors with the cluster center. If the distance between a predicted pseudorange error and the cluster center exceeds a predetermined threshold, we identify the corresponding satellite measurement as faulty

and exclude it from further processing. Conversely, if the distance is within the threshold, we consider the corresponding satellite measurement as normal and retain it for further calculations.
Once the faulty measurements are detected and excluded, the position and velocity of the receiver can be calculated using the remaining measurements. This can be achieved through least squares estimation, where the reliable pseudorange measurements are used to estimate the vehicle position and velocity accurately.

2.5 Loosely Coupled GPS/IMU/VO Fusion scheme

By combining the GPS, IMU, and VO data, we can provide the estimation of the vehicle position, velocity, and attitude. This fusion is achieved using a loosely coupled scheme in the framework of the Extended Kalman Filter (EKF).
The state vector for the EKF is defined as follows:

$$\boldsymbol{X} = \begin{bmatrix} \delta \boldsymbol{r}^{e}_{3\times1} & \delta \boldsymbol{v}^{e}_{3\times1} & \delta \boldsymbol{\varphi}_{3\times1} & \boldsymbol{b}_{g3\times1} & \boldsymbol{b}_{a3\times1} & \boldsymbol{s}_{g3\times1} & \boldsymbol{s}_{a3\times1} \end{bmatrix}^{T} \quad (9)$$

where $\boldsymbol{X}$ represents the state vector; $\delta \boldsymbol{r}^{e}_{3\times1}$, $\delta \boldsymbol{v}^{e}_{3\times1}$, and $\delta \boldsymbol{\varphi}_{3\times1}$ denote the three-dimensional position error vector, velocity error vector and attitude error vector of IMU, respectively; $\boldsymbol{b}_{g3\times1}$ and $\boldsymbol{b}_{a3\times1}$ represent the three-axis bias of the gyroscope and accelerometer; $\boldsymbol{s}_{g3\times1}$ and $\boldsymbol{s}_{a3\times1}$ are the three-axis scale factor of the gyroscope and accelerometer, respectively.
The state transition equation for the GPS/IMU/VO Kalman filter can be expressed as:

$$\boldsymbol{X}_k = \boldsymbol{\Phi}_{k,k-1}\boldsymbol{X}_{k-1} + \boldsymbol{w}_{k-1} \quad (10)$$

where, $\boldsymbol{X}_{k-1}$ and $\boldsymbol{X}_k$ are the state vectors at time epoch k-1 and k, respectively; $\boldsymbol{\Phi}_{k,k-1}$ represents the state transition matrix from time epoch k-1 to k; $\boldsymbol{w}_{k-1}$ represents the process noise at time epoch k-1.
The measurement equation of the system is given by:

$$\boldsymbol{Z}_k = \begin{bmatrix} \boldsymbol{p}_{IMU\_k} - \boldsymbol{p}_{GPS\_k} \\ \boldsymbol{v}_{IMU\_k} - \boldsymbol{v}_{GPS\_k} \\ \boldsymbol{v}_{IMU\_k} - \boldsymbol{v}_{VO\_k} \end{bmatrix} = \boldsymbol{H}\boldsymbol{X}_k + \boldsymbol{\eta}_k \quad (11)$$

where $\boldsymbol{Z}_k$ represents the measurement vector of the time epoch k; $\boldsymbol{H}$ is the measurement mapping matrix; $\boldsymbol{\eta}_k$ denotes the measurement noise at time epoch k; $\boldsymbol{p}_{IMU\_k}$ and $\boldsymbol{v}_{IMU\_k}$ represent the position and velocity derived from the IMU at time epoch k, respectively; $\boldsymbol{p}_{GPS\_k}$ and $\boldsymbol{v}_{GPS\_k}$ are the position and velocity solutions of GPS after FDE at time epoch k, respectively; $\boldsymbol{v}_{VO\_k}$ represents the position derived from the VO at time epoch k.
In the loosely coupled GPS/IMU/VO fusion system, if the number of available GPS signals after FDE is less than 4, in order to guarantee the performance of the system, we incorporate VO data to integrate with IMU. The observation equation is expressed as:

$$\boldsymbol{Z}_k = \boldsymbol{v}_{IMU\_k} - \boldsymbol{v}_{VO\_k} = \boldsymbol{H}\boldsymbol{X}_k + \boldsymbol{\eta}_k \quad (12)$$

After confirming the state transition equation and the measurement equation, the state vector can then be estimated using the Kalman filter. The Kalman filtering procedure can be divided into two stages as follows:
Prediction stage:

$$\hat{\boldsymbol{X}}_{k,k-1} = \boldsymbol{\Phi}_{k,k-1}\hat{\boldsymbol{X}}_{k-1} \quad (13)$$

$$\boldsymbol{P}_{k,k-1} = \boldsymbol{\Phi}_{k,k-1}\boldsymbol{P}_{k-1}\boldsymbol{\Phi}_{k,k-1}{}^{T} + \boldsymbol{Q}_{k-1} \quad (14)$$

Update stage:

$$\boldsymbol{K}_k = \boldsymbol{P}_{k,k-1}\boldsymbol{H}_k{}^{T}\left(\boldsymbol{H}_k\boldsymbol{P}_{k,k-1}\boldsymbol{H}_k{}^{T} + \boldsymbol{R}_k\right)^{-1} \quad (15)$$

$$\boldsymbol{P}_k = \left(\boldsymbol{I} - \boldsymbol{K}_k\boldsymbol{H}_k\right)\boldsymbol{P}_{k,k-1} \quad (16)$$

$$\hat{\boldsymbol{X}}_k = \hat{\boldsymbol{X}}_{k,k-1} + \boldsymbol{K}_k\left(\boldsymbol{Z}_k - \boldsymbol{H}_k\hat{\boldsymbol{X}}_{k,k-1}\right) \quad (17)$$

where, $\hat{\boldsymbol{X}}_{k-1}$ denotes the system state vector estimate at time epoch k-1, corresponding to covariance matrix $\boldsymbol{P}_{k-1}$; $\hat{\boldsymbol{X}}_{k,k-1}$ represents the predicted state vector, corresponding to covariance matrix $\boldsymbol{P}_{k,k-1}$; $\boldsymbol{Q}_{k-1}$ is the system noise matrix; $\boldsymbol{K}_k$ is the kalman gain; $\boldsymbol{R}_k$ denotes the measurement noise matrix; $\hat{\boldsymbol{X}}_k$ represents the system state vector estimate at time epoch k, corresponding to covariance matrix $\boldsymbol{P}_k$; $\boldsymbol{I}$ is an identity matrix.
Next, the estimated position, velocity and attitude from the IMU are corrected using the state vector. This final estimation provides an improved estimation of the vehicle position, velocity, and attitude. It can be output and utilized to aid in predicting the vehicle position in the next epoch.

3. EXPERIMENT AND RESULTS

To validate the proposed algorithm, a field test was carried out in Nanjing, Jiangsu, China. The experimental vehicle and equipment are depicted in Figure 2. During the test, raw GNSS measurements were collected using a BDStar Navigation C520-AT GNSS receiver with a sampling rate of 10Hz. The raw IMU data were collected using a micro-electro-mechanical system (MEMS) IMU, STIM300, with a sampling rate of 125Hz. The parameters of the STIM300 are provided in Table 1. Images were captured using an Intel RealSense D455 binocular depth stereo camera with a resolution of 848×480 and a sampling rate of 30Hz. For reference during the dynamic test, a Honeywell HGuide n580 satellite/inertial navigation device was used. The ground truth was obtained through post-processing in the Inertial Explore software, using a tightly coupled integration mode. The corresponding IMU parameters are provided in Table 2.

Accelerometer	Bias instability	0.05 mg
	Random walk noise	0.06 m/s/sqrt(hr)
Gyroscope	Bias instability	0.5 deg/hr
	Random walk noise	0.15 deg/sqrt(hr)

Table 1. Parameters of STIM300.

Accelerometer	Bias instability	0.025 mg
	Random walk noise	0.03 m/s/sqrt(hr)
Gyroscope	Bias instability	0.25 deg/hr
	Random walk noise	0.15 deg/sqrt(hr)

Table 2. Parameters of N580.

Figure 2. Experimental vehicle and experimental equipment.

The experiment was conducted in a dense-urban environment near Nanjing South Railway Station. The experimental route and partial experimental scenes are depicted in Figure 3. As illustrated in the figure, there are many obstacles along the driving trajectory, including skyscrapers and elevated bridge. These obstacles have the potential to block and reflect satellite signals, leading to significant GPS outages and multipath effects. So it is essential to mitigate the multipath effects to improve the navigation performance in these urban environments.

The number of visible satellites and PDOP value before and after FDE are presented in Figure 4. As depicted in the figure, our proposed algorithm demonstrates the capability to identify multiple faulty satellites and can operate effectively even when the number of available satellites is less than 5. After excluding the detected faulty satellites, the PDOP value may increase, indicating a decrease in the geometric quality of the satellite constellation. However, the GPS positioning results will become more accurate and reliable without the influence of contaminated measurements.

In order to assess the performance of the proposed GPS/IMU/VO integrated navigation system with FDE algorithm, the proposed algorithm is compared with the traditional GPS/IMU/VO integrated algorithm. Figure. 5 illustrates the trajectories calculated by the two algorithms. It is evident from the figure that the positioning results obtained from the proposed algorithm are closer to the reference trajectory compared to the traditional algorithm, particularly in complex environments.

The position, velocity and attitude errors, calculated from the proposed algorithm and comparison algorithm, are shown in

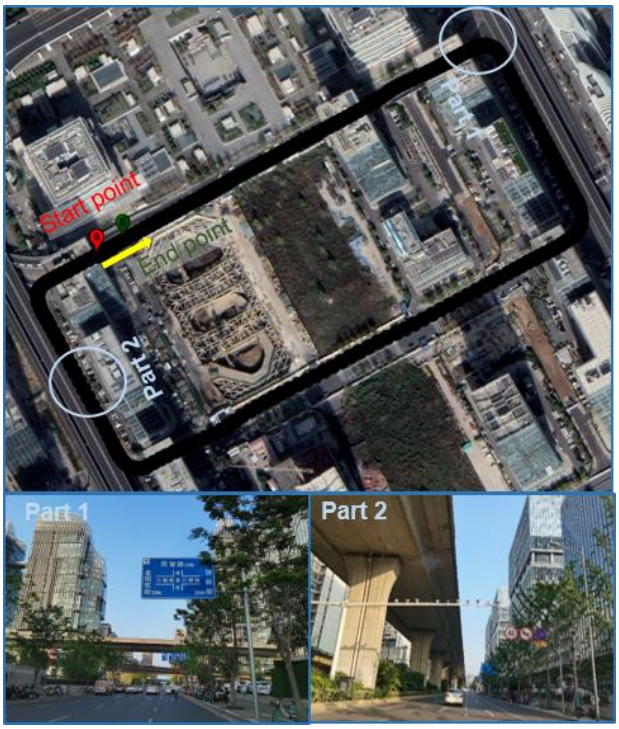

Figure 3. The experimental route and partial experimental scenes.

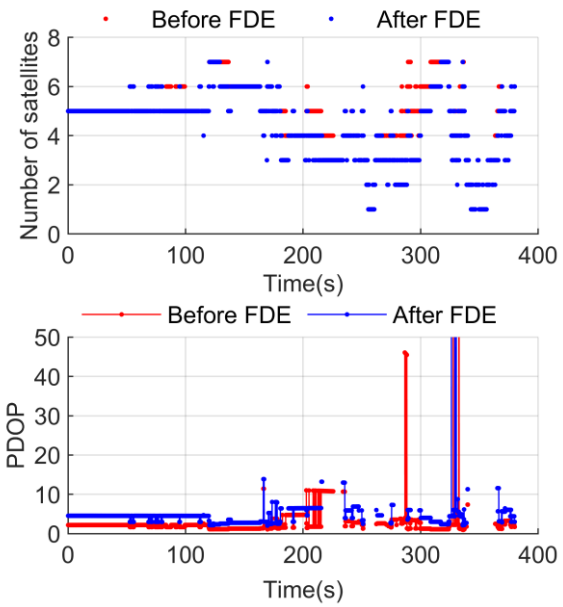

Figure 4. Number of visible satellites and PDOP value before and after FDE.

Figure 6-8, respectively. The accuracy of the two algorithms is further analyzed using Root Mean Square Error (RMSE), and the results are presented in Tables 3-5 for position, velocity, and attitude, respectively.

Based on the results, it is evident that the proposed GPS/IMU/VO integration system with FDE algorithm significantly improves the vehicle positioning accuracy. The 3D positioning RMSE is reduced to 11.18m, representing a substantial improvement compared to the traditional GPS/IMU/VO fusion with an RMSE of 35.18 m. The

positioning accuracies in the north, east, and down directions are greatly enhanced by 74.1%, 75.1%, and 19.8%, respectively. The improvement in positioning accuracy in the down direction is relatively small due to the utilization of NHC in the traditional GPS/IMU/VO fusion. Moreover, a significant enhancement is observed in the overall 3D Root Mean Square Error (RMSE) of velocity, showcasing an improvement of approximately 60.0% when contrasting the proposed solutions with the conventional integration approach. This demonstrates the superior accuracy and reliability of the proposed algorithm in velocity estimation. Regarding attitude estimation, the proposed GPS/IMU/VO integration outperforms the traditional algorithm, particularly in heading estimation. The estimated heading accuracy of the proposed algorithm is 1.855 degrees, representing a substantial 79.1% improvement compared to the traditional GPS/IMU/VO integration solution, which has an estimated heading accuracy of 8.888 degrees. These improvements demonstrate the effectiveness of the proposed FDE algorithm in enhancing vehicle navigation performance in urban environments, providing more accurate and reliable position, velocity, and attitude estimations.

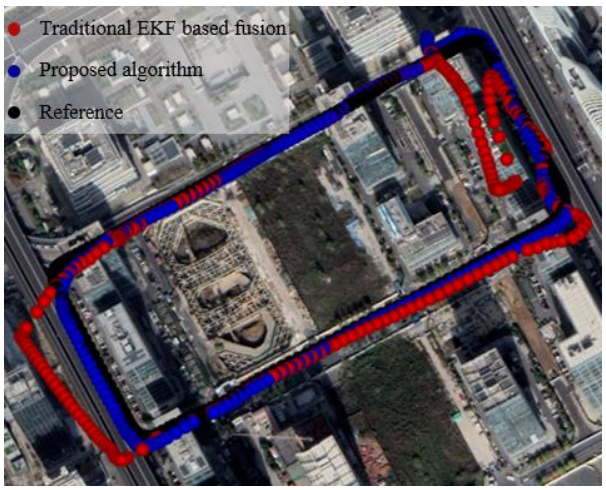

Figure 5. Trajectory comparison for traditional integrated algorithm and the proposed algorithm.

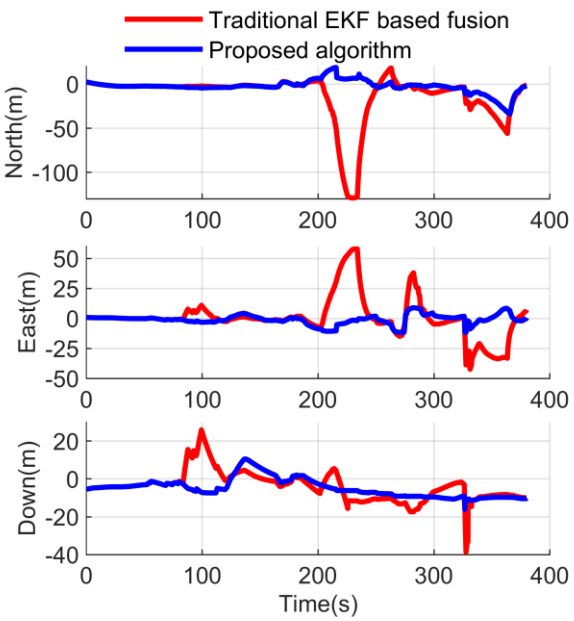

Figure 6. Comparison of position error.

Algorithm	Position RMSE (m)				
	North	East	Down	Horizontal	3D
EKF	29.75	16.68	8.65	34.1	35.18
Proposed algorithm	7.72	4.16	6.93	8.77	11.18
Improvement	74.1%	75.1%	19.8%	74.3%	68.2%

Table 3. Position RMSE results comparison.

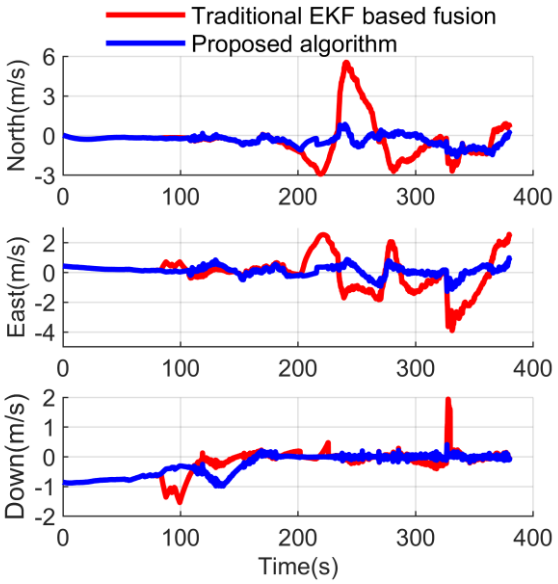

Figure 7. Comparison of velocity error.

Algorithm	Velocity RMSE (m/s)		
	North	East	Down
EKF	1.45	1.11	0.49
Proposed algorithm	0.51	0.34	0.44
Improvement	64.6%	69.2%	11.4%

Table 4. Velocity and attitude RMSE results comparison.

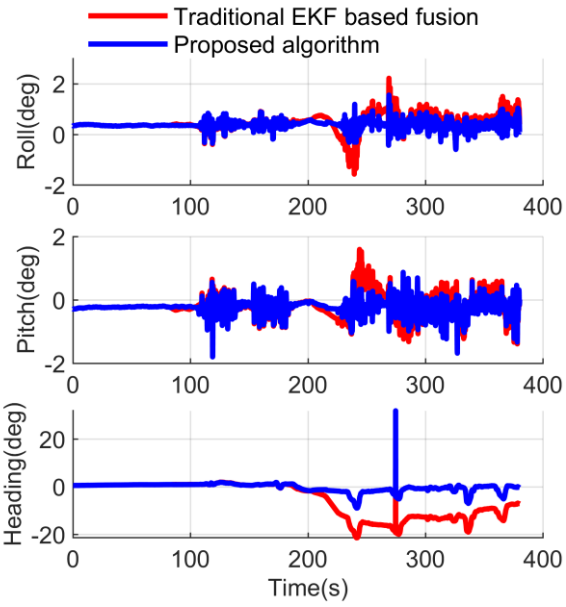

Figure 8. Comparison of attitude error.

Algorithm	Attitude RMSE (degree)		
	Pitch	Roll	Heading
EKF	0.383	0.556	8.888
Proposed algorithm	0.310	0.410	1.855
Improvement	19.0%	26.3%	79.1%

Table 5. Attitude RMSE results comparison.

4. CONCLUSION

This paper proposes a novel FDE algorithm for GPS/IMU/VO integration in urban environments to enhance vehicle navigation. The proposed algorithm utilizes IMU and VO data to predict pseudorange errors and incorporates Hierarchical Clustering algorithm to identify faulty satellite signals based on the predicted pseudorange error. The integration system utilizes IMU and VO data not only for fusion with GPS data to provide navigation results but also to assist in the FDE process within the GPS system. A field test was conducted in a dense urban environment to evaluate the performance of the proposed algorithm. The experimental results demonstrate that the GPS/IMU/VO integration with the proposed FDE algorithm significantly improve the navigation accuracy. The RMSEs of 3D positioning, velocity, and attitude are 11.18m, 0.76m/s, and 1.925 degrees, respectively. These results represent a 68.2% improvement in positioning accuracy, a 60.0% improvement in velocity estimation, and a 78.4% improvement in attitude estimation compared to the traditional GPS/IMU/VO integration approach. These results highlight the effectiveness of the proposed algorithm in mitigating NLOS or multipath errors and improving the accuracy and reliability of vehicle navigation in challenging urban environments.

ACKNOWLEDGEMENTS

This work was supported in part by the National Natural Science Foundation of China (Grant No. 42222401, 41974033, 42174025), the Natural Science Foundation of Jiangsu Province (Grant No. BK20211569), and Fundamental Research Funds for the Central Universities (Grant No. NE2022006 and xcxjh20220726). (Corresponding author: Rui Sun.)

REFERENCES

Blanch, J., Walter, T., Enge, P., et al., 2012: Advanced RAIM user algorithm description: Integrity support message processing, fault detection, exclusion, and protection level calculation. Proceedings of the 25th International Technical Meeting of The Satellite Division of the Institute of Navigation (ION GNSS 2012), 2828-2849.

Chen, X., He, D., Pei, L., 2020: BDS B1I multipath channel statistical model comparison between static and dynamic scenarios in dense urban canyon environment. Satellite Navigation, 1(1), 1-16.

Fagnant, D.J., Kockelman, K., 2015: Preparing a nation for autonomous vehicles: Opportunities, barriers and policy recommendations. Transportation Research Part A: Policy and Practice, 77, 167–181.

Feng, S., Ochieng, W.Y., Walsh, D., et al., 2006: A measurement domain receiver autonomous integrity monitoring algorithm, Gps Solutions, 10, 85-96.

Guermah, B., GHAZI, H.E., Sadiki, T., Guermah, H., 2018: A robust GNSS LOS/multipath signal classifier based on the fusion of information and machine learning for intelligent transportation systems, 2018 IEEE International Conference on Technology Management, Operations and Decisions (ICTMOD), Marrakech, Morocco, 94-100.

Hsu, L.T., 2017: GNSS multipath detection using a machine learning approach, 2017 IEEE 20th International Conference on Intelligent Transportation Systems (ITSC), Yokohama, Japan, 1-6.

Lee, Y.C., Young, C., 1986: Analysis of Range and Position Comparison Methods as a Means to Provide GPS Integrity in the User Receiver, Proceedings of the 42nd Annual Meeting of The Institute of Navigation, Seattle, Washington, 1-4.

MacGougan, G., Lachapelle, G., Klukas, R., et al., 2002: Performance analysis of a stand-alone high-sensitivity receiver. GPS Solutions, 6: 179-195.

Meguro, J., Murata, T., Takiguchi, J., et al., 2009: GPS multipath mitigation for urban area using omnidirectional infrared camera, IEEE Transactions on Intelligent Transportation Systems, 10(1), 22-30.

Nielsen, F. (2016): Hierarchical Clustering. In: Introduction to HPC with MPI for Data Science. Springer, Cham.

Parkinson, B.W., Axelrad, P., 1998: Autonomous GPS integrity monitoring using the pseudorange residual. Navigation, 35(2): 255-274.

Peyraud, S., Bétaille, D., Renault, S., et al., 2013: About non-line-of-sight satellite detection and exclusion in a 3D map-aided localization algorithm. Sensors, 13(1), 829-847.

Sturza, M.A., 1988: Navigation system integrity monitoring using redundant measurements. Navigation, 35(4): 483-501.

Sun, R., Wang, G., Zhang, W., et al., 2020: A gradient boosting decision tree based GPS signal reception classification algorithm, Applied Soft Computing, 86, 105942.

Sun, R., Wang, J., Cheng, Q., et al., 2021: A new IMU-aided multiple GNSS fault detection and exclusion algorithm for integrated navigation in urban environments, GPS Solutions, 25, 1-17.

Yang, H., Fan, X., Shi, P., et al., 2015: Nonlinear control for tracking and obstacle avoidance of a wheeled mobile robot with nonholonomic constraint, IEEE Transactions on Control Systems Technology, 24(2), 741-746.